Structure, Vol. 13, 1635–1642, November, 2005, ©2005 Elsevier Ltd All rights reserved. DOI 10.1016/j.str.2005.07.018

Activation Process of [NiFe] Hydrogenase Elucidated by High-Resolution X-Ray Analyses: Conversion of the Ready to the Unready State

Hideaki Ogata,[1,2,8] Shun Hirota,[3,4,8,*] Asuka Nakahara,[1] Hirofumi Komori,[1,5] Naoki Shibata,[1,5] Tatsuhisa Kato,[6] Kenji Kano,[7] and Yoshiki Higuchi[1,5,*]

[1]Department of Life Science
Graduate School of Life Science
University of Hyogo and Himeji Institute of Technology
3-2-1 Koto
Kamigori-cho
Ako-gun
Hyogo 678-1297
Japan

[2]Max-Planck-Institut für Bioanorganische Chemie
D-45470 Mülheim an der Ruhr
Germany

[3]Department of Physical Chemistry
21st Century COE Program
Kyoto Pharmaceutical University
5 Nakauchi-cho
Misasagi
Yamashina-ku
Kyoto 607-8414
Japan

[4]PRESTO
JST
Kawaguchi
Saitama 332-0012
Japan

[5]RIKEN Harima Institute/SPring-8
1-1-1 Koto
Mikazuki-cho
Sayo-gun
Hyogo 679-5248
Japan

[6]Department of Chemistry
Josai University
1-1 Keyakidai
Sakado
Saitama 350-0295
Japan

[7]Division of Applied Life Sciences
Graduate School of Agriculture
Kyoto University
Sakyo
Kyoto 606-8502
Japan

Summary

Hydrogenases catalyze oxidoreduction of molecular hydrogen and have potential applications for utilizing dihydrogen as an energy source. [NiFe] hydrogenase has two different oxidized states, Ni-A (unready, exhibits a lag phase in reductive activation) and Ni-B (ready). We have succeeded in converting Ni-B to Ni-A with the use of Na_2S and O_2 and determining the high-resolution crystal structures of both states. Ni-B possesses a monatomic nonprotein bridging ligand at the Ni-Fe active site, whereas Ni-A has a diatomic species. The terminal atom of the bridging species of Ni-A occupies a similar position as C of the exogenous CO in the CO complex (inhibited state). The common features of the enzyme structures at the unready (Ni-A) and inhibited (CO complex) states are proposed. These findings provide useful information on the design of new systems of biomimetic dihydrogen production and fuel cell devices.

Introduction

Since fossil energy resources will be exhausted in the near future, it is an imperative issue to seek new energy sources. Microorganisms have an effective system for utilizing hydrogen for metabolism by using hydrogenases. A detailed understanding of the mechanism of enzymatic hydrogen activation at the molecular level can be provided by the structure of the active site in hydrogenase. This detailed structural knowledge is required for the creation of new systems of biomimetic dihydrogen production and fuel cell devices for the next generation.

Hydrogenases have very unique active sites and are classified into several groups according to the metal composition of the active sites: [Fe]-only, [NiFe], and [NiFeSe] hydrogenases (Vignais and Colbeau, 2004; Darensbourg et al., 2000). The hydrogenase previously referred to as metal free has recently been shown to contain a functional iron (Shima et al., 2004). The active site of [NiFe] hydrogenase in the oxidized state consists of Ni and Fe atoms coordinated to four cysteinyl sulfur and four nonprotein ligands (Armstrong, 2004; Stein and Lubitz, 2002). The nonprotein ligands are assigned as two CN^- groups, one CO bound to the Fe atom, and a bridging O or OH between the Ni and Fe atoms for the enzyme from *Desulfovibrio gigas* (Happe et al., 1997; Pierik et al., 1999). In contrast, the bridging ligand has shown stronger electron density than that corresponding to an ordinary oxygen atom, and the possible presence of a sulfur ligand has been proposed (Higuchi et al., 1997; Ogata et al., 2002). The bridging ligand has been shown to disappear upon reduction of the enzyme (Higuchi et al., 1999; Higuchi and Yagi, 1999). We have recently demonstrated that, in the CO-related structures, the Ni and $S\gamma$(Cys546) atoms show flexibility, which suggested that these two atoms play a key role during the initial H_2 binding process (Ogata et al., 2002). [NiFe] hydrogenase also possesses one $[Fe_3S_4]^{1+/0}$ cluster with a relatively high midpoint potential (−70 mV) and two $[Fe_4S_4]^{2+/1+}$ clusters with lower midpoint potentials (−290 and −340 mV, respectively) (Higuchi et al., 1997; Teixeira et al., 1989; Volbeda et al., 1995), and the EPR signal of the oxidized $[Fe_3S_4]^+$ cluster is detected at g = 2.01 at low temperatures (Albracht et al., 1983; Cammack et al., 1987).

*Correspondence: hig@sci.u-hyogo.ac.jp (Y.H.); hirota@mb.kyoto-phu.ac.jp (S.H.)

[8]These authors contributed equally to this work.

Two different oxidized forms of [NiFe] hydrogenase, Ni-A and Ni-B, have been identified on the basis of EPR signals (Albracht et al., 1983), although it is not clear whether these states are physiologically relevant. High O_2 tensions resulted in a population of enzyme molecules with a high proportion of Ni-B, whereas low O_2 tensions resulted primarily in Ni-A (van der Zwaan et al., 1990). However, experimental control of the conversion between the two states has been difficult. The Ni-A state needs at least 1 hr of incubation at room temperature to show activity in the presence of H_2, but the Ni-B state is readily activated with H_2 (Fernandez et al., 1985). Although there have been several reports on the differences between the two states (van der Zwaan et al., 1990; Carepo et al., 2002; Trofanchuk et al., 2000; Bleijlevens et al., 2001), the origin of these differences has not been clearly elucidated. For example, the interaction of O_2 with the enzyme was investigated with the use of ^{17}O, which showed that an oxygen species must be present in close proximity to the Ni atom in both the Ni-A and Ni-B states (van der Zwaan et al., 1990). ^{17}O ENDOR studies on the Ni-A state in $H_2{}^{17}O$ obtained after one reduction/reoxidation cycle showed that a solvent-derived oxygen is a ligand to Ni and that the bridging ligand in the Ni-A state is an oxygenic species (O^{2-} or OH^-) (Carepo et al., 2002). To clarify the differences between the two oxidized states, Ni-A and Ni-B, and to elucidate the mechanism of the transition between them on the basis of their three-dimensional structures, we have succeeded in converting the enzyme from the Ni-B state to the Ni-A state with the use of Na_2S and O_2. By comparing the high-resolution crystal structures of the [NiFe] hydrogenase in the Ni-A, Ni-B, as-purified, H_2-reduced, and CO bound forms, we identified not only the differences between the structures of the active site, but also elucidated the essential structural features of the unready state of the enzyme.

Results and Discussion

Changes in EPR Signals of the Ni-B State by Interaction with Na_2S

The as-purified [NiFe] hydrogenase from *D. v*. Miyazaki F showed an EPR spectrum that was a mixture of typical Ni-A (g = 2.01, 2.24, 2.32) and Ni-B (g = 2.01, 2.16, 2.33) peaks, with an excess of the Ni-B peaks (Figure 1A). By anaerobic addition of 50 mM Na_2S to the as-purified enzyme containing a mixture of the Ni-A and Ni-B states, the $[Fe_3S_4]^+$ EPR signal at g = 2.01 observed at 20 K decreased rapidly and was almost undetectable after 1 min at room temperature (Figure 1B), whereas the EPR signal of the Ni site observed at 90 K exhibited no significant changes, except for the disappearance of the signal at g = 2.13 (Figure 1A, a → b). The g = 2.13 signal is often observed for the [NiFe] hydrogenase from *D. v*. Miyazaki F. The reason for this anomalous g value is currently unknown, but it may be attributed to the structural fluctuations of the modified species found at $S\gamma$ of Cys546.

The disappearance of the $[Fe_3S_4]^+$ EPR signal corresponds to the reduction of the Fe_3S_4 cluster to the $[Fe_3S_4]$ state. An EPR signal for a thiyl radical, the electron transfer product from HS^-, was not observed, probably due to the slow formation and high reactivity of this radical. The reduction time was slowed at higher viscosity by the addition of 33% (v/v) 2-methyl-2,4-pentanediol (MPD). The absorption around 450–460 nm decreased upon addition of Na_2S to the as-purified enzyme, although the absorption around 400 nm did not decrease completely (data not shown). The results show that the iron-sulfur clusters, or at least some part of them, remain oxidized after interaction with Na_2S.

While the $[Fe_3S_4]^+$ EPR signal decreased within 1 min, the Ni-B signals started to convert to new EPR signals (g = 2.00, 2.14, and 2.29; Ni-B′) within 6 min, without significant changes in the Ni-A signals (Figure 1A, b → c). Actually, no change was observed in the Ni EPR signals with the addition of Na_2S to the purified Ni-A enzyme, although the $[Fe_3S_4]^+$ EPR signal disappeared (data not

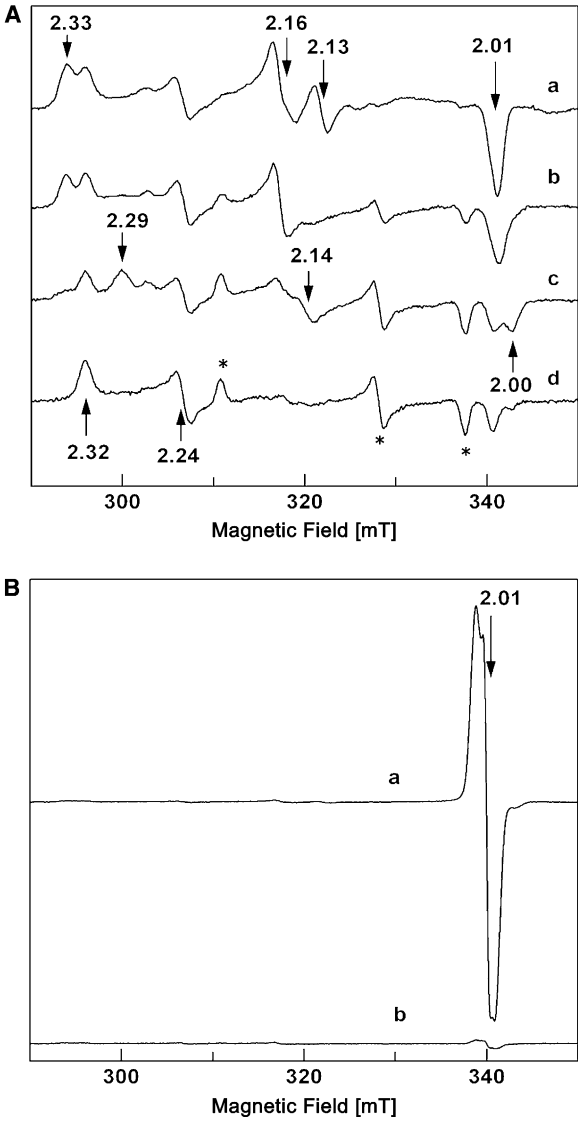

Figure 1. EPR Spectra of [NiFe] Hydrogenase from *D. v*. Miyazaki (A and B) (A) 90 and (B) 20 K. (a) As-purified, (b) 1 min after addition of Na_2S, (c) 6 min after addition of Na_2S (50 mM), and (d) after exposure to air. Experimental conditions: frequency, 9.592 GHz; power, (A) 2 and (B) 0.2 mW; enzyme concentration, 220 μM; 25 mM Tris-HCl (pH 7.4). Asterisks correspond to the signals of the denatured protein, which disappears by dialysis.

shown). By interaction of the new Ni-B′ species with O_2, the Ni-B′ EPR signals converted to the Ni-A signals (Figure 1A, c → d). The enzyme obtained after treatment with Na_2S was repurified to remove Na_2S. Although the enzyme obtained after treatment with Na_2S could be activated in the presence of methylviologen and H_2, it required a prolonged incubation time longer than 40 min. This result also supports the interpretation of the conversion from the ready Ni-B state to the unready Ni-A state. The Ni-A enzyme activity after activation was comparable to that of the Ni-B enzyme. The rate of transition did not differ significantly in D_2O buffer. The Ni-A state did not convert back to the Ni-B state by dialysis or by placing the Na_2S-treated enzyme at 4ºC for 3 days. By addition of Na_2S to the as-purified enzyme under air, the EPR signals of the Ni-B state gradually converted to those of the Ni-A state, which was accomplished in about an hour at room temperature.

During the interaction of the new Ni-B′ species with oxygen, the $[Fe_3S_4]^+$ EPR signal was generated to a small extent within a few minutes, and then the signal started to decrease again (data not shown). These results indicate that decrease in the new Ni-B′ species at the active site by a trace of molecular oxygen is coupled with intramolecular electron transfer from the Fe_3S_4 cluster to the active site. The generated $[Fe_3S_4]^+$ signal finally disappeared after a few minutes, due to rereduction of $[Fe_3S_4]^+$ by Na_2S. By addition of 33% (v/v) MPD, the initial increase of the $[Fe_3S_4]^+$ EPR signal by reaction with oxygen was larger because of the decrease in the rereduction rate of $[Fe_3S_4]$ by Na_2S (see text above). The Ni-B′ state, however, should be very reactive against O_2, since Na_2S functions as a strong oxygen quencher.

Crystal Structures of the Ni-A and Ni-B States

The pure Ni-A state could be obtained with the addition of Na_2S, and the resulting X-ray structures were refined at a resolution of 1.04–1.50 Å with R values (free R values [Brünger, 1992]) between 0.101 and 0.123 (0.123–0.167). As a result of the SHELXL refinement, two of the intrinsic nonprotein diatomic ligands of Fe (L2 and L3) were able to be assigned as CN and CO, respectively, on the basis of their atomic parameters. Even by X-ray analyses at ultra-high resolution it was difficult to identify the atomic species of the L1 ligand, which was suggested as CN for some enzymes. Summaries of the data collection and processing statistics are shown in Table 1 and Table S1 (see the Supplemental Data available with this article online).

Two aspects of the structure at the active site are quite noteworthy. The first aspect is the size of the nonprotein bridging ligand, and the second one is the modification of the sulfur atoms of the cysteine ligands (Cys84 and Cys546). The Ni-A structure shows a large electron density peak at the site of the nonprotein bridging ligand (Figure 2A). The concave shape at the center region and the size of the density strongly suggest that this ligand is a diatomic species. In contrast, the corresponding density peaks of the Ni-B (Figure 2B) and as-purified states (Figure S1A, see the Supplemental Data available with this article online) are apparently smaller (about half) than that of the Ni-A state, suggesting that a monatomic species is situated at the bridging ligand site (Higuchi et al., 1997), which is in agreement with previously reported observations on the structure of the as-purified enzyme. The sizes of the nonprotein bridging ligand of Ni-A and Ni-B are similar to those found in the structures from *Desulfovibrio gigas* and *Desulfovibrio fructosovorans* enzymes (Volbeda et al., 2005). Electron density is not observed in the H_2-reduced state between the two metals (Figure S1B). The diatomic and monatomic species are designated XA1-XA2 and XB1 for the Ni-A and Ni-B states, respectively (XA1 and XB1 are the atoms directly coordinated to both the Ni and Fe atoms). When oxygen atoms are assigned to these atoms, the distance between XA1 and XA2 in the Ni-A state in the refined structure is 1.57 Å. This O—O distance is clearly longer than that found in a dioxygen

Table 1. Summary of the X-Ray Crystallographic Data of the Ni-A and Ni-B Structures

Crystal	Ni-A	Ni-B
Data Collection and Refinement Statistics		
Space group: $P2_12_12_1$		
Cell constants (Å)		
a	98.069	98.162
b	125.966	125.924
c	66.380	66.441
Resolution (Å)[a]	1.04 (1.10–1.04)	1.40 (1.48–1.40)
Completeness (%)[a]	98.0 (92.5)	99.4 (97.4)
R_{merge}[a]	0.069 (0.455)	0.069 (0.376)
R value (>σ [F])[a]	0.108 (0.248)	0.122 (0.237)
R_{free} (>σ [F])	0.140	0.164
Rms deviation from ideality		
Bond length (Å)	0.016	0.010
Bond angle (º)	0.031	0.027
Mean coordination error from Luzzati plot (Å)	0.04	0.07
Number of reflections	352,706	149,696
Number of parameters	65,493	63,591
Reflections/parameters	5.4	2.4
Water molecules	995	834
2-methyl-2,4-pentanediol	4	0
Structural Parameters of the Ni-Fe Active Site		
Ni-Fe distance (Å)	2.80	2.69
Nonprotein bridging ligand		
Angle (º) Ni–XA(B)1–Fe[b]	90.6 (91.4)	88.9 (92.6)
Distance (Å)		
Ni–XA(B)1[b]	1.70 (1.69)	1.67 (1.55)
Fe–XA(B)1[b]	2.20 (2.19)	2.14 (2.12)
XA1–XA2[b]	1.57 (1.57)	—
Q		
XA(B)1[b]	0.99 (0.49)	0.57 (0.31)
XA2[b]	0.59 (0.54)	—
B (Å^2)		
XA(B)1[b]	12.9 (13.1)	12.5 (12.1)
XA2[b]	17.3 (16.7)	—
Cys546		
Distance (Å) Sγ–X546[b]	1.77	1.50
Q X546[b]	0.39	0.94
B (Å^2) X546[b]	11.2	23.9
Cys84		
Distance (Å) Sγ–X84[b]	1.58	—
Q X84[b]	0.53	—
B (Å^2) X84[b]	11.0	—

[a] Values in parentheses are for the outer shell of the resolution range.
[b] Values for XA1, XB1, XA2, X546, and X84 are for oxygen species, whereas those in parentheses are for sulfur species.

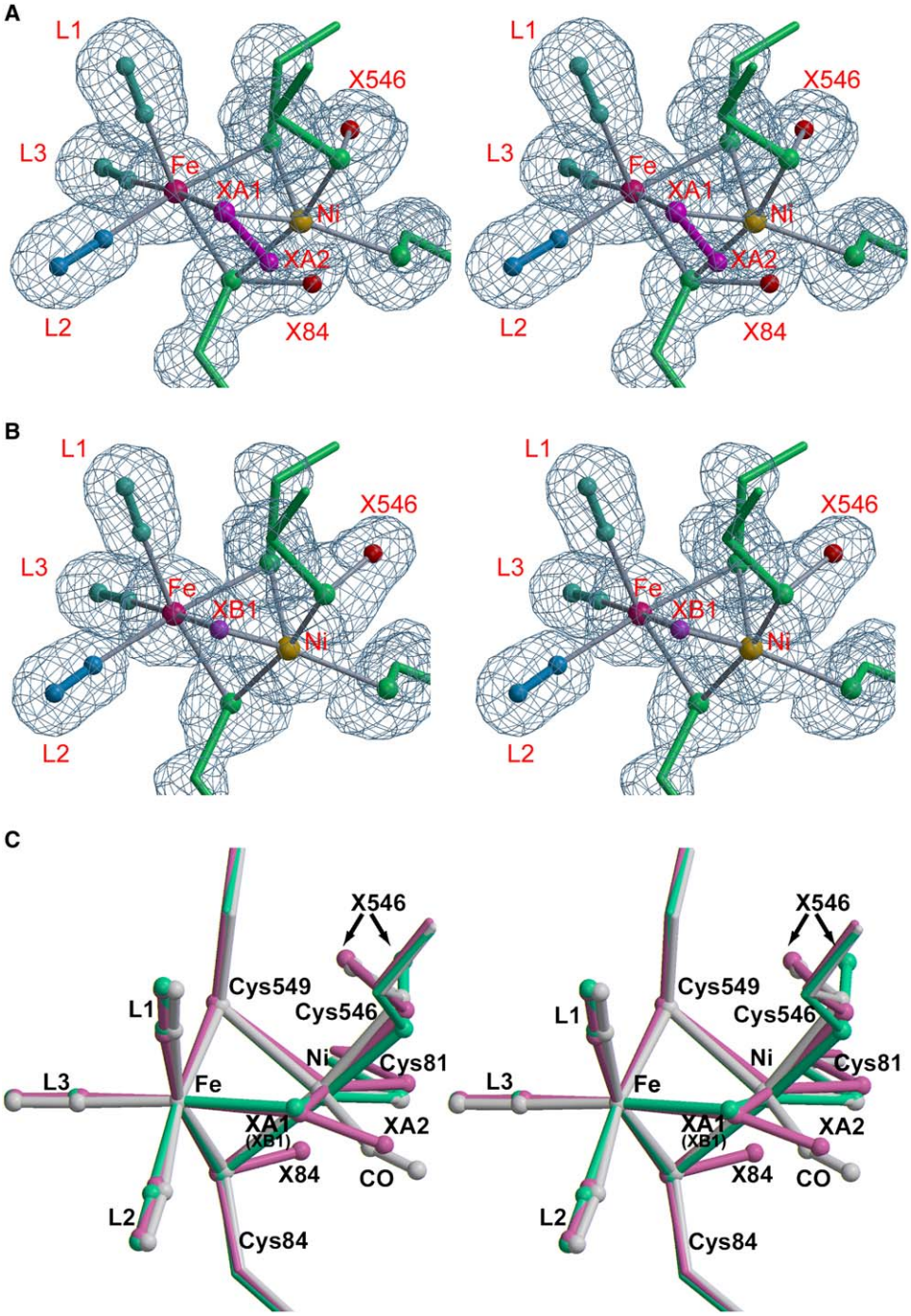

Figure 2. Structures of the Ni-Fe Active Site

(A and B) Stereodiagrams of the electron density distribution (omit map) around the Ni-Fe active site with a ball-and-stick model of the (A) Ni-A and (B) Ni-B structures.

(C) Superimposition of the structures of the Ni-A (red), Ni-B (green), and CO complex (gray, Ogata et al., 2002) states. XA2 of Ni-A occupies a similar position as C of the exogenous CO of the CO complex. X546s of the Ni-A and CO complex structures are shifted toward the Ni atom compared to that of the Ni-B structure (see text). L1, L2, and L3 indicate nonprotein diatomic ligands of the Fe atom, and they are tentatively assigned as CO, CN, and CO, respectively, on the basis of the refined atomic parameters. XA1-XA2 (Ni-A) and XB1 (Ni-B) are nonprotein bridging ligands between the Ni and Fe atoms. X84 and X546 are additional atomic species attached to Sγ of Cys84 and Cys546, respectively.

species, such as O═O and H_2O_2 (1.2–1.4 Å). The relatively long O—O distance can be attributed to a hydroperoxide species coordinated to two metals, since a similar O—O distance is lengthened to 1.46 Å for a mononuclear hydroperoxide copper complex (Wada et al., 1998). Recently, a hydroperoxide bridge has been suggested to be a coordination scheme at the Ni-Fe active site in the Ni-A state by electrochemical (Lamle et al., 2004) and crystallographic studies (Volbeda et al., 2005). Ni-A was formed under conditions in

which there were not enough electrons to reduce O_2 to H_2O (Lamle et al., 2004), and molecular oxygen is partially reduced to hydroperoxide when two reducing equivalents are available. Additional oxidation of Cys(SH) to Cys(S=O), however, was observed during the conversion from Ni-B to Ni-A. The Ni–Fe distance in the Ni-B state (2.69 Å) is similar to that of the as-purified enzyme. The longer Ni–Fe distance in the Ni-A state (2.80 Å) may be caused by the larger bridging ligand between the two metals.

The second structural difference is the modified feature of the cysteine sulfur ligands. Both Cys84 (bridging ligand) and Cys546 (terminal ligand) show residual electron density peaks in the Ni-A state (Figure 2A), whereas Cys546 showed a residual peak in the Ni-B (Figure 2B), as-purified (Figure S1A), H_2-reduced (Figure S1B), and CO bound (COC crystal [Ogata et al., 2002]) states. These residual peaks are attributed to be modifications of the nearest atoms (Sγ546 and Sγ549), considering the connection feature of the electron density distribution. When an oxygen species was assigned to these densities (named X84 and X546 for Cys84 and Cys546, respectively), the refinements all converged normally. The X546–Sγ546 and X84–Sγ84 distances ranged from 1.46 to 1.77 Å in all structures. The location of X546, however, can be divided into two groups: Group-A (Ni-A and CO complex) and Group-B (Ni-B, as-purified, and H_2-reduced). By comparison with Group-B, X546 in Group-A is shifted about 1.0 Å toward Sγ of Cys549, resulting in reduction of the X546–Ni distance by about 0.5 Å (Figure 2C and Figure S1C). As a result, X546, Sγ546, Sγ549, and the Ni atom in the Ni-A state form a tightly packed structure within a distance of 2.50 Å (X546–Ni = 2.26 Å, Ni–Sγ546 = 2.12 Å, Sγ546–X546 = 1.77 Å, X546–Sγ549 = 2.40 Å, Ni–Sγ549 = 2.48 Å). X84 (Ni-A) also shows a notable feature. It is located near the Ni atom with a distance of about 1.80 Å; thus, X84 sits at the location nearest the Ni atom (X84–Ni = 1.77 Å, Ni–Sγ84 = 2.53 Å, Sγ84–X84 = 1.58 Å, X84–Sγ81 = 2.21 Å, Ni–Sγ81 = 2.21 Å). Since X84 pushes the Sγ atom of Cys81 away from the Ni atom, it also contributes to the larger Ni–Fe distance in the Ni-A state. Interestingly, the XA2 species in the Ni-A state sits in a similar position as that of the carbon atom of the exogenous CO in the CO complex (Figure 2C). It should be emphasized that the structure around the Ni atom in the Ni-A state surprisingly resembles that in the CO complex, although the atomic species are different. The XA2 atom may also block the pathway of dihydrogens and/or protons. In fact, it is located at the dead end of the hydrophobic pathways, which are connected by the cavities from the molecular surface to the Ni atom. The modification of the coordinated sulfur atoms only in the Ni-A structure reported here has also been reported by Volbeda et al. (2005).

Assignment of the atomic species of the bridging ligand (they were assigned as monatomic so far) has been controversial, since the size of the electron density peak considerably differs from one structure to another (Higuchi et al., 1997, 1999; Volbeda et al., 1996; Matias et al., 2001). Refinement with an oxygen species for XB1 in the Ni-B state and XA2 in the Ni-A state converged normally (XB1: Q = 0.57, averaged B [B_{ave}] = 12.5 Å^2; XA2: Q = 0.59, averaged B [B_{ave}] = 17.3 Å^2). The occupancy factor Q of XA1 in the Ni-A state obtained by the refinement with an oxygen species is relatively large (Q = 0.99), whereas it converged to a normal value (Q = 0.49) when the oxygen atom of XA1 was replaced with a sulfur atom. The parameters of the additional atoms (X546 and X84) attached to the Sγ atom of the cysteine ligands all converged in the normal range by assignment of an oxygen species (Table 1 and Table S1). This is in accordance with the previously reported EPR experiments with ^{17}O (O_2 and H_2O), which strongly suggests that there must be an oxygen species near the Ni atom (van der Zwaan et al., 1990; Carepo et al., 2002). All modified features, such as XA1, XA2, XB1, X84, and X546 (if it is also attached to the Ni atom), are candidates for the oxygen species, which affect the electronic state of the Ni atom at the active site. They can be assigned as an oxygen species on the basis of the refined atomic parameters discussed above even though there are still some anomalous features concerning the Q factors. The enzyme, however, always liberates H_2S when the oxidized enzyme is reduced with an electron carrier under an H_2 atmosphere (Higuchi and Yagi, 1999). The amounts of the liberated H_2S in the Ni-A, as-purified, and Ni-B states were in a molar ratio to enzyme of 0.62, 0.24, and 0.08, respectively. These results indicate that a sulfur species exists near the active site, suggesting that some of the nonprotein ligand atoms, XA1, XA2, XB1, X84, and X546, may be a sulfur species. The electron density peaks at X84 and X546 for the CO complex (COC crystal) (Ogata et al., 2002) and the as-purified (Higuchi et al., 1997), and H_2-reduced (Higuchi et al., 1999) structures disappeared, presumably due to successive exposure to an intense X-ray beam at the synchrotron. Considering these results, X84 and X546 are the most probable candidates for the source of the liberated H_2S.

Mechanism for Transition of Ni-B to the Ni-A State by Na_2S

From EPR and crystallographic studies, we propose the following reactions for the transition of the Ni-B state to the Ni-A state by the addition of Na_2S (Figure 3). The $[Fe_3S_4]^+$ cluster is reduced to $[Fe_3S_4]$ by intermolecular interaction with Na_2S, whereas the species bound to Sγ of Cys546 in fluctuated conformations has settled in a stable conformation. The Ni-B state is converted to a newly detected state (Ni-B′) with g = 2.00, 2.14, and 2.29 by interaction with Na_2S. The magnitude of the EPR shift by treatment with Na_2S was comparable with the differences in the signals of Ni-B and Ni-A, where the character of the bridging ligand is different. We, therefore, suggest a small perturbation in the ligands of Ni between Ni-B and Ni-B′. In the new Ni-B′ state, HS^- might bind to the metal at the active site. For example, the sulfur atom can bind to the iron atom of an organometallic compound (Curtis et al., 1995). Although only an intensity decrease in the Ni EPR signal has been reported during the reduction of the $[Fe_3S_4]$ cluster by lowering of the reduction potential (Teixeira et al., 1989), the active site may change its structure by the reduction of the $[Fe_3S_4]$ cluster; thus, Ni-B′ could also be Ni-B with a reduced $[Fe_3S_4]$ cluster. The new Ni-B′ species interacts with dioxygen to produce the Ni-A state, which has a diatomic ligand (probably a dioxygen) at the bridging site with a positional shift of

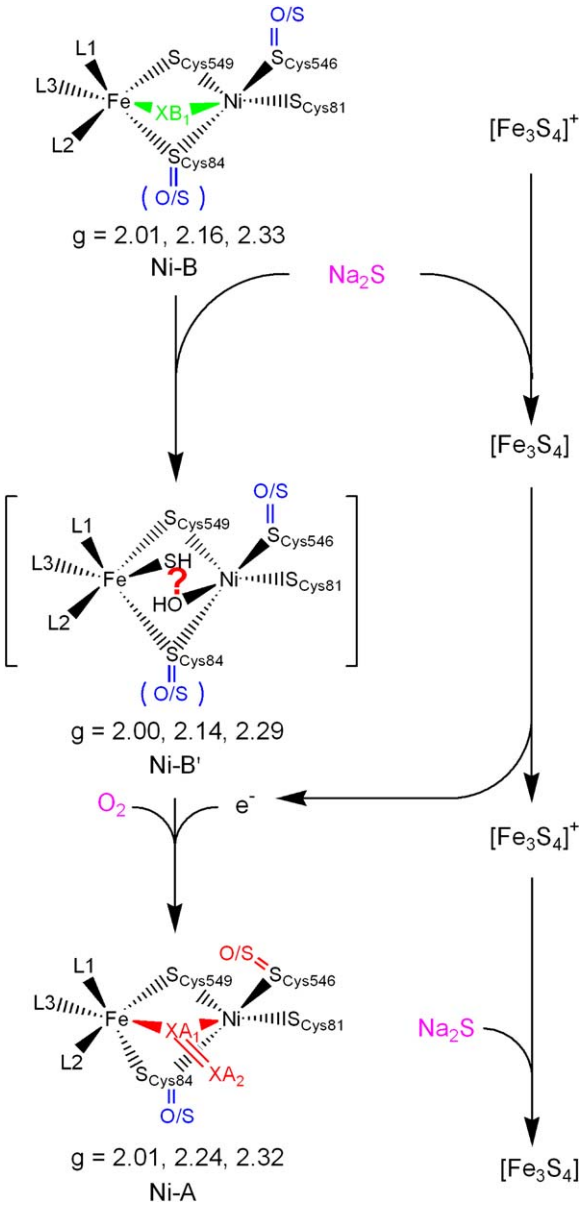

Figure 3. Proposed Scheme for the Conversion of the Ni-B State of [NiFe] Hydrogenase to the Ni-A State by Addition of Na_2S

The Ni-B state has a monatomic bridging ligand, XB1 (probably an oxygen species), whereas the produced Ni-A state has a diatomic ligand, XA1-XA2 (probably a dioxygen), at the bridging site. The X546 atom (modified species of the sulfur atom of Cys546) of Ni-A is shifted from the position of that of Ni-B toward the Ni atom. The most probable candidates of the atomic species of XA1, XA2, XB1, X84, and X546 are all oxygen species; however, sulfur species are also possible for XA1, XB1, X84, and X546 (see the text for details). The hypothetical structure of the Ni-B′ state is shown.

X546 at Sγ546. During production of the Ni-B state, an electron of the $[Fe_3S_4]$ cluster is consumed to produce $[Fe_3S_4]^+$, and the produced $[Fe_3S_4]^+$ is rereduced with Na_2S. Transition of the enzyme in the Ni-B state to the Ni-A state occurs by (1) conversion of the Ni active site to a new Ni-B′ species by Na_2S addition and (2) reaction of the produced Ni-B′ species with O_2 by consuming an electron at the Fe_3S_4 site. These results support a dioxygen species as the bridging ligand for the Ni-A state.

The unique, to our knowledge, structure of the Ni-A state presented here, which surprisingly resembles that of the CO-inhibited state, shows the essential features of the unready (inhibited) state of the enzyme. In other words, the inhibition of the catalytic reaction of [NiFe] hydrogenase is attributed to the XA2, X84, and X546 species in the Ni-A state, and the spatial position of XA2 must be vacant for the reaction with the substrate. These findings are crucially important to elucidate the activation and/or inhibition mechanism of the active site of [NiFe] hydrogenase and may be useful to design and develop model compounds of artificial hydrogenases.

Experimental Procedures

Sample Preparation

Isolation and purification of the oxidized [NiFe] hydrogenase from *D. v*. Miyazaki F with an excess of the Ni-B state have been carried out according to the protocol described previously (Higuchi et al., 1987). The enzyme solution was concentrated by using a Centricon-30 filter and was stored at 77 K for later use. The Ni-B state was made by reduction of the enzyme with methylviologen and hydrogen, subsequently oxidizing it with an excess amount of O_2. The Ni-A state was obtained by the addition of Na_2S. Na_2S was dissolved in 25 mM Tris-HCl (pH 7.4), and the pH value and concentration of the Na_2S solution were adjusted to 7.4 and 500 mM, respectively, with concentrated HCl and the buffer solution. The 500 mM Na_2S solution was added to the as-purified enzyme immediately after the pH adjustment (final Na_2S concentration, 50 mM). The as-purified enzyme automatically converts to the Ni-A state if it is exposed to air for 5 min. After the enzyme solutions of the Ni-A and Ni-B states were prepared, the enzyme was further purified by anion exchange chromatography with DEAE Toyopearl 650S in order to remove the denatured protein components.

EPR and Electrochemical Measurements

EPR spectra were measured at 20 and 90 K with a Bruker E500 spectrometer. The temperature was controlled by a helium flow cryostat (Oxford Instruments Model ESR910) and a cryostat controller (Oxford Instruments Model ITC500). The $[Fe_3S_4]^+$ and Ni signals were measured at 20 and 90 K, respectively. The frequencies and microwave power for the measurements were 9.592 GHz and 0.2 mW (20 K) and 2 mW (90 K), respectively. [NiFe] hydrogenase was dissolved in 25 mM Tris-HCl buffer (pH 7.4) and was added with pH-adjusted Na_2S solution. Changes in the EPR spectra of the as-purified enzyme in the presence of Na_2S were measured under air or under strictly prepared anaerobic conditions by using a vacuum line and sealing the sample tube with a burner.

Hydrogenase activity was measured with a Clark-type oxygen electrode (Central Science). The activity of 20 nM enzyme was measured in the presence of 1.6 mM methyl viologen and 0–250 mM Na_2S under an H_2 atmosphere.

Crystallization, Data Collection, and Structure Refinement

Crystals of the Ni-A, Ni-B, as-purified, and H_2-reduced states were prepared by the methods described previously (Higuchi et al., 1987, 1997, 1999). The crystals grown from the enzyme solution of the Ni-A state were confirmed to have the typical Ni-A EPR signals (data not shown). We have previously found that solution EPR spectra are essentially the same as the single crystal EPR spectra for the oxidized enzyme used in this study (Trofanchuk et al., 2000). X-ray diffraction data sets for Ni-A (BL44B2), Ni-B (BL40B2), as-purified (BL41XU), and H_2-reduced (BL44B2) were collected at 100 K in the dark at SPring-8 (Hyogo, Japan) at a wavelength of 0.7000 Å. Diffraction images were indexed with the program MOSFLM (Leslie, 1991) and scaled with SCALA of the CCP4 package (CCP4, 1994). For crystals diffracted beyond the resolution of 1.3 Å, diffraction data sets in the low- and high-resolution ranges were collected separately. Initial refinement was carried out by using the coordinates of the H_2-reduced structure (PDB code 1H2R) with CNS (Brünger et al., 1998). In the final stages, alternative conformations and anisotropic B factors were refined with SHELXL (Sheldrick and Schneider, 1997).

The coordinated atoms at the active site were all refined without any stereochemical restraints in order to obtain the real features of the coordination geometry. The occupancy factors (Q) of the atoms comprising the active site were also refined at the final stage of the SHELXL refinement. Model building was done with XFIT (McRee, 1999), and the figures were prepared with MOLSCRIPT (Kraulis, 1991), BOBSCRIPT (Esnouf, 1997), and RASTER3D (Merritt and Murphy, 1994).

Measurements of H_2S Liberated from the Oxidized Enzyme by H_2 Reduction

As-purified, Ni-A, and Ni-B hydrogenase solutions were dialyzed for 24 hr against 25 mM Tris-HCl (pH 6.7). Pure N_2 was bubbled through the outer solution during the dialysis in order to remove the extra H_2S, which may remain in the enzyme solution after Ni-A preparation with Na_2S. Each dialyzed enzyme solution was concentrated to 0.5–1.0 mM, transferred to a vial (1.0 ml), sealed, and kept at 4ºC until use. The outer solution of the dialysis was also measured as a blank solution. Measurements and calculations of the amount of the liberated H_2S from the activated enzyme with an electron carrier (5 mM methylviologen) were carried out according to the protocol described previously (Higuchi and Yagi, 1999). H_2S was analyzed by using a Shimadzu gas chromatograph with Ar as a carrier gas at 70ºC. The total amount of H_2S (nmol) contained in the reaction vial was calculated by the equation: $H_2S_{total} = [H_2S]_{gas}(V_{gas} + V_{liq}\ \alpha_{pH}\ T/273)$, where α_{pH}, V_{gas}, and V_{liq} stand for $\alpha\ (1 + 10^{pH\text{-}pKa})$, the volumes of the gas phase (0.8 ml), and the volumes of the liquid phase (0.2 ml), respectively. As a result, H_2S_{total} was calculated by using the equation: $H_2S_{total} = 1.49 \times [H_2S]_{gas}$ (pH 6.7 at 310 K).

Supplemental Data

Supplemental Data including the structures of the Ni-Fe active site and the summary of the X-ray crystallographic data of the as-purified and H_2-reduced structures are available at http://www.structure.org/cgi/content/full/13/11/1635/DC1/.

Acknowledgments

We would like to express our sincere thanks to Drs. A. Kikuchi and Y. Shiro of RIKEN Harima Institute/SPring-8 and Dr. H. Axelrod of the Joint Center for Structural Genomics at the Stanford Synchrotron Radiation Laboratory for their helpful discussions. This work was partially supported by Grants-in-Aid for Scientific Research by Ministry of Education, Culture, Sports, Science and Technology, Japan (Priority Areas, No.164041242 [S.H.] and 16074214 [Y.H.]), the 21st COE Programs (S.H. and Y.H.), the National Project on Protein Structural and Functional Analyses (Y.H.), the Japanese Aerospace Exploration Agency project (Y.H.), the Project for Development of a Technological Infrastructure for Industrial Bioprocesses on R&D of New Industrial Science and Technology Frontiers by Ministry of Economy, Trade and Industry and New Energy and Industrial Technology Development Organization (Y.H.), Japan Society for the Promotion of Science (Category C, No. 16550149 [S.H.] and Category B, No. 14380317 [Y.H]), Japanese Science and Technology Agency (S.H.), the research fund by Hyogo Science Technology Association (Y.H.), and the Showa Shell Sekiyu Foundation for Promotion of Environmental Research (S.H.).

Received: May 6, 2005
Revised: July 22, 2005
Accepted: July 23, 2005
Published: November 8, 2005

References

Albracht, S.P.J., Kalkman, M.L., and Slater, E.C. (1983). Magnetic interaction of nickel (111) and the iron-sulphur hydrogenase from *Chromatium vinosum*. Biochim. Bhiophys. Acta *724*, 309–316.

Armstrong, F.A. (2004). Hydrogenases: active site puzzles and progress. Curr. Opin. Chem. Biol. *8*, 133–140.

Bleijlevens, B., Faber, B.W., and Albracht, S.P.J. (2001). The [NiFe] hydrogenase from allochromatium vinosum studied in EPR-detectable states: H/D exchange experiments that yield new information about the structure of the active site. J. Biol. Inorg. Chem. *6*, 763–769.

Brünger, A.T. (1992). The free R value: a novel statistical quantity for accessing the accuracy of crystal structures. Nature *355*, 472–477.

Brünger, A.T., Adams, P.D., Clore, G.M., DeLano, W.L., Gros, P., Grosse-Kunstleve, R.W., Jiang, J.-S., Kuszewski, J., Nilges, M., Pannu, N.S., et al. (1998). Crystallography & NMR system: a new software suite for macromolecular structure determination. Acta Crystallogr. D Biol. Crystallogr. *54*, 905–921.

Cammack, R., Patil, D.S., Hatchikian, E.C., and Ferández, V.M. (1987). Nickel and iron-sulfur centers in *Desulfovibrio gigas* hydrogenase-electron-spin-resonance spectra, redox properties and interactions. Biochim. Biophys. Acta *912*, 98–109.

Carepo, M., Tierney, D.L., Brondino, C.D., Yang, T.C., Pamplona, A., Telser, J., Moura, I., Moura, J.J.G., and Hoffman, B.M. (2002). ^{17}O ENDOR detection of a solvent-derived Ni-(OHx)-Fe bridge that is lost upon activation of the hydrogenase from *Desulfovibrio gigas*. J. Am. Chem. Soc. *124*, 281–286.

CCP4 (Collaborative Computational Project, Number 4) (1994). The CCP4 suite: programs for protein crystallography. Acta Crystallogr. D Biol. Crystallogr. *50*, 795–800.

Curtis, M.D., Riaz, U., Curnow, O.J., Kampf, J.W., Rheingold, A.L., and Haggerty, B.S. (1995). Molecular structures of the bimetallic sulfido clusters, $Cp'_2Mo_2Co_2S_4(CO)_2$, $Cp'_2Mo_2Co_2S_4(PPh_3)(CO)$, $Cp'_2Mo_3CoS_4(CO)$, $Cp'_2Mo_3FeS_4(SH)$. Organometallics *14*, 5337–5343.

Darensbourg, M.Y., Lyon, E.J., and Smee, J.J. (2000). The bio-organometallic chemistry of active site iron in hydrogenases. Coord. Chem. Rev. *206–207*, 533–561.

Esnouf, R.M. (1997). An extensively modified version of molscript that includes generally enhanced colouring capabilities. J. Mol. Graph. Model. *15*, 132–134.

Fernandez, V.M., Hatchikian, E.C., and Cammack, R. (1985). Properties and reactivation of two different deactivated forms of *Desulfovibrio gigas* hydrogenase. Biochim. Biophys. Acta *832*, 69–79.

Happe, R.P., Roseboom, W., Pierik, A.J., Albracht, S.P.J., and Bagley, K.A. (1997). Biological activation of hydrogen. Nature *385*, 126.

Higuchi, Y., and Yagi, T. (1999). Liberation of hydrogen sulfide during the catalytic action of *Desulfovibrio* hydrogenase under the atmosphere of hydrogen. Biochem. Biophys. Res. Commun. *255*, 295–299.

Higuchi, Y., Yasuoka, N., Kakudo, M., Katsube, Y., Yagi, T., and Inokuchi, H. (1987). Single crystals of hydrogenase from *Desulfovibrio vulgaris* Miyazaki F. J. Biol. Chem. *262*, 2823–2825.

Higuchi, Y., Yagi, T., and Yasuoka, N. (1997). Unusual ligand structure in Ni-Fe active center and an additional Mg site in hydrogenase revealed by high resolution X-ray structure analysis. Structure *5*, 1671–1680.

Higuchi, Y., Ogata, H., Miki, K., Yasuoka, N., and Yagi, T. (1999). Removal of the bridging ligand atom at the Ni-Fe active site of [NiFe] hydrogenase upon reduction with H_2, as revealed by X-ray structure analysis at 1.4 Å resolution. Structure *7*, 549–556.

Kraulis, P.J. (1991). MOLSCRIPT: a program to produce both detailed and schematic plots of protein structures. J. Appl. Crystallogr. *24*, 946–950.

Leslie, A.G.W. (1991). Integration of macromolecular diffraction data. Acta Crystallogr. D Biol. Crystallogr. *55*, 1696–1702.

Lamle, S.E., Albracht, S.P.J., and Armstrong, F.A. (2004). Electrochemical potential-step investigations of the aerobic interconversions of [NiFe]-hydrogenase from allochromatium vinosum: insights into the puzzling difference between unready and ready oxidized inactive states. J. Am. Chem. Soc. *126*, 14899–14909.

Matias, P.M., Soares, C.M., Saraiva, L.M., Coelho, R., Morais, J., Gall, J.L., and Carrondo, M.A. (2001). [NiFe] hydrogenase from *Desulfovibrio desulfuricans* ATCC 27774: gene sequencing, three-dimensional structure determination and refinement at 1.8 Å and modeling studies of its interaction with the tetrahaem cytochrome c_3. J. Biol. Inorg. Chem. *6*, 63–81.

McRee, D.E. (1999). XtalView/Xfit - a versatile program for manipulating atomic coordinates and electron density. J. Struct. Biol. *125*, 156–165.

Merritt, E.A., and Murphy, M.E.P. (1994). Raster3D Version 2.0 - a program for photorealistic molecular graphics. Acta Crystallogr. *D50*, 869–873.

Ogata, H., Mizoguchi, Y., Mizuno, N., Miki, K., Adachi, S., Yasuoka, N., Yagi, T., Yamauchi, O., Hirota, S., and Higuchi, Y. (2002). Structural studies of the carbon monoxide complex of [NiFe] hydrogenase from *Desulfovibrio vulgaris* Miyazaki F: suggestion for the initial activation site for dihydrogen. J. Am. Chem. Soc. *124*, 11628–11635.

Pierik, A.J., Roseboom, W., Happe, R.P., Bagley, K.A., and Albracht, S.P.J. (1999). Carbon monoxide and cyanide as intrinsic ligands to iron in the active site of [NiFe]-hydrogenases. $NiFe(CN)_2CO$, biology's way to activate H_2. J. Biol. Chem. *274*, 3331–3337.

Sheldrick, G.M., and Schneider, T.R. (1997). SHELXL: high-resolution refinement. Methods Enzymol. *277*, 319–343.

Shima, S., Lyon, E.J., Sordel-Klippert, M., Kauss, M., Kahnt, J., Thauer, R.K., Steinbach, K., Xie, X., Verdier, L., and Griesinger, C. (2004). The cofactor of the iron-sulfur cluster free hydrogenase Hmd: structure of the light-inactivation product. Angew. Chem. Int. Ed. Engl. *43*, 2547–2551.

Stein, M., and Lubitz, W. (2002). Quantum chemical calculations of [NiFe] hydrogenase. Curr. Opin. Chem. Biol. *6*, 243–249.

Teixeira, M., Moura, I., Xavier, A., Moura, J.J.G., LeGall, J., DerVartanian, D.V., Harry Peck, J., and Huynh, B.-H. (1989). Redox intermediates of *Desulfovibrio gigas* [NiFe] hydrogenase generated under hydrogen. Mössbauer and EPR characterization of the metal centers. J. Biol. Chem. *264*, 16435–16450.

Trofanchuk, O., Stein, M., Gessner, C., Lendzian, F., Higuchi, Y., and Lubitz, W. (2000). Single crystal EPR studies of the oxidized active site of [NiFe] hydrogenase from *Desulfovibrio vulgaris* Miyazaki F. J. Biol. Inorg. Chem. *5*, 36–44.

van der Zwaan, J.W., Coremans, J.M.C.C., Bouwens, E.C.M., and Albracht, S.P.J. (1990). Effect of $^{17}O_2$ and ^{13}CO on EPR spectra of nickel in hydrogenase from *Chromatium vinosum*. Biochim. Biophys. Acta *1041*, 101–110.

Vignais, P.M., and Colbeau, A. (2004). Molecular biology of microbial hydrogenases. Curr. Issues Mol. Biol. *6*, 159–188.

Volbeda, A., Charon, M.-H., Piras, C., Hatchikian, E.C., Frey, M., and Fontecilla-Camps, J.C. (1995). Crystal structure of the nickel-iron hydrogenase from *Desulfovibrio gigas*. Nature *373*, 580–587.

Volbeda, A., Garcin, E., Piras, C., de Lacey, A.L., Fernandez, V.M., Hatchikian, E.C., Frey, M., and Fontecilla-Camps, J.C. (1996). Structure of the [Ni-Fe] hydrogenase active site: evidence for biologically uncommon Fe ligands. J. Am. Chem. Soc. *118*, 12989–12996.

Volbeda, A., Martin, L., Cavazza, C., Matho, M., Faber, B.W., Roseboom, W., Albracht, S.P.J., Garcin, E., Rousset, M., and Fontecilla-Camps, J.C. (2005). Structural differences between the ready and unready oxidized states of [NiFe] hydrogenases. J. Biol. Inorg. Chem. *10*, 239–249.

Wada, A., Harata, M., Hasegawa, K., Jitsukawa, K., Masuda, H., Mukai, M., Kitagawa, T., and Einaga, H. (1998). Structural and spectroscopic characterization of a mononuclear hydroperoxo-copper(II) complex with tripodal pyridylamine ligands. Angew. Chem. Int. Ed. Engl. *37*, 798–799.

Accession Numbers

The coordination data of Ni-A, Ni-B, as-purified, and H_2-reduced [NiFe] hydrogenases have been deposited in the Protein Data Bank with the accession codes of 1WUI, 1WUJ, 1WUK, and 1WUL, respectively.